J. Fluid Mech. (1997), *vol.* 342, *pp.* 159–177. Printed in the United Kingdom

Finite-amplitude equilibrium states in plane Couette flow

By A. CHERHABILI AND U. EHRENSTEIN

Université Lille 1, Laboratoire de Mécanique de Lille URA CNRS 1441, Bd. P. Langevin, F-59655 Villeneuve d'Ascq Cedex, France

(Received 20 June 1996 and in revised form 2 December 1996)

A numerical bifurcation study in plane Couette flow is performed by computing successive finite-amplitude equilibrium states, solutions of the Navier–Stokes equations. Plane Couette flow being linearly stable for all Reynolds numbers, first two-dimensional equilibrium states are computed by extending nonlinear travelling waves in plane Poiseuille flow through the Poiseuille–Couette flow family to the plane Couette flow limit. The resulting nonlinear states are stationary with a spatially localized structure; they are subject to two-dimensional and three-dimensional secondary disturbances. Three-dimensional disturbances dominate the dynamics and three-dimensional stationary equilibrium states bifurcating at criticality on the two-dimensional equilibrium surface are computed. These nonlinear states, periodic in the spanwise direction and spatially localized in the streamwise direction, are computed for Reynolds numbers (based on half the velocity difference between the walls and channel half-width) close to 1000. While a possible relationship between the computed solutions and experimentally observed coherent structures in turbulent plane Couette flow has to be assessed, the present findings reinforce the idea that subcritical transition may be related to the existence of finite-amplitude states which are (unstable) fixed points in a dynamical systems formulation of the Navier–Stokes system.

1. Introduction

While linear stability analyses are capable of predicting the onset of transition from a laminar to a turbulent flow state in many fluid systems, they fail when applied to shear flows with a subcritical transition behaviour. The linear stage of transition is bypassed for example in plane Poiseuille flow where transition has been observed for Reynolds numbers much lower than the value for linear instability. Concerning subcritical transition in shear flows, plane Couette flow may be considered as a kind of prototype. Indeed plane Couette flow, that is the flow in a channel induced by the relative motion of two infinite parallel walls, is known to be linearly stable for all Reynolds numbers, as shown by Romanov (1973) who analysed the spectrum of the linearized Navier–Stokes operator. Hence, despite its simple analytical expression, plane Couette flow is a challenging fluid system for transition studies.

Since the pioneering experimental investigation of Reichardt (1956) until quite recently only few experimental studies of transition in plane Couette flow seemed to be available, mainly due to experimental difficulties. Reichardt (1956) reported turbulent plane Couette flow for Reynolds numbers, expressed in terms of channel half-width and half the velocity difference between the walls, of 750. More recently, introducing wall roughness, Aydin & Leutheusser (1991) determined a critical Reynolds number of 300. Numerical simulations of turbulent plane Couette flow have been performed for

instance by Andersson, Bech & Kristoffersen (1992) who provide turbulent statistics for Reynolds numbers of about 1300. The turbulent structure in plane Couette flow using both numerical and experimental data has been investigated recently by Bech *et al.* (1995). Concentrating on low-Reynolds-number regions, flow visualization experimental results have been reported by Tillmark & Alfredsson (1992). These authors located the lowest Reynolds number for which turbulence can be sustained at approximately 360. Using finite-amplitude perturbations by a transverse jet flow injection into the laminar flow Daviaud, Hegseth & Bergé (1992) determined the minimum Reynolds number for subcritical transition at 370. Measurements of critical amplitudes for finite-amplitude perturbations have led to a critical Reynolds number of 325 (Dauchot & Daviaud 1995*a*). The direct numerical simulation of turbulent spots for a Reynolds number of 375 performed by Lundbladh & Johansson (1991) are in general agreement with these experimental findings.

Hence there is numerical (cf. also Orszag & Kells 1980) and experimental evidence that transition driven by finite-amplitude perturbations in plane Couette flow prevails for low Reynolds numbers. However, the transition process in plane Couette flow is far from being understood. Plane Couette flow being stable for infinitesimal disturbances, a bifurcation analysis from primary to subsequent instabilities fails. Investigating the linear and weakly nonlinear stability of the Poiseuille–Couette flow family parameterized by the wall velocity, Cowley & Smith (1985) showed that weakly nonlinear solutions bifurcate from infinity for wall velocities above a cut-off value. The possibility of transient energy growth for subcritical shear flows including plane Couette flow has been advanced by Reddy & Henningson (1993). Linear transient amplification is analysed in the mathematical context of non-normal operators, and this theory is capable of providing bounds for threshold amplitudes (cf. Kreiss, Lundbladh & Henningson 1994).

While linear transient energy growth can possibly trigger nonlinearities leading to transition (cf. Baggett, Driscoll & Trefethen 1995) the question of the existence and basin of attraction of nonlinear states is certainly intimately related to transition (cf. Waleffe 1995). The search for equilibrium states with increasing spatial and/or temporal complexity (Saffman 1983) has been undertaken for instance for the pressure-driven plane Poiseuille channel flow. Since the numerical investigations of Zahn *et al.* (1974) and Herbert (1977) it is now well established that two-dimensional steady waves in plane Poiseuille flow exist for Reynolds numbers of 2900, which is about half the value for linear instability ($R_c \approx 5772$). Computations of those nonlinear states as well as secondary stability results have been reported by Pugh & Saffman (1988) and Soibelman & Meiron (1991). Three-dimensional finite-amplitude waves bifurcating from the two-dimensional equilibrium surface have been computed by Ehrenstein & Koch (1991) for Reynolds numbers of 1000, close to measured transitional values.

Those numerical bifurcation studies cannot be applied straightforwardly to plane Couette flow due to the absence of a primary (linear) instability. To circumvent this difficulty Lerner & Knobloch (1988) introduced a small defect in an (inviscid) two-dimensional plane Couette flow leading to linear instability. This approach has been generalized by Dubrulle & Zahn (1991) who added viscous effects. Instead of producing a more or less artificial linear instability an alternative procedure is to use a continuation strategy starting from known nonlinear states for a flow configuration somehow connected to plane Couette flow. Extending finite-amplitude solutions for a circular Couette system between co-rotating cylinders with a narrow gap to the case with zero average rotation rate Nagata (1990) succeeded in computing three-dimensional nonlinear states for Reynolds numbers close to 125. Bifurcation sequences

in a Bénard–Couette problem have been produced by Clever & Busse (1992) leading to plane Couette flow as limiting case (for a zero Rayleigh number).

An alternative approach proposed by Milinazzo & Saffman (1985) is to connect, by continuation in the wall velocity, finite-amplitude states in plane Poiseuille flow to the zero-pressure-gradient plane Couette flow limit. In a previous work (Cherhabili & Ehrenstein 1995) we reconsidered this idea focusing on the question of existence of two-dimensional finite-amplitude states in plane Couette flow, a question that has given rise to some controversy in the past. The most striking result is that the nonlinear travelling waves in plane Poiseuille flow evolve into solitary-like stationary states for plane Couette flow. The two-dimensional states reported in Cherhabili & Ehrenstein (1995) are only a first stage of the description of the nonlinear process. Indeed those states are unstable to secondary disturbances leading to subsequent bifurcations possibly related to the transition process. Analogous bifurcation analyses have been performed for plane Poiseuille flow (Pugh & Saffman 1988; Soibelman & Meiron 1991; Ehrenstein & Koch 1991) or for the Blasius boundary-layer flow (Koch 1992; Ehrenstein & Koch 1995).

The present paper is organized as follows. Section 2 contains the governing equations and the solution procedure. In §3 we summarize the results concerning the two-dimensional equilibrium states reported in Cherhabili & Ehrenstein (1995). Section 4 is devoted to the stability analysis of these nonlinear states with respect to two-dimensional as well as three-dimensional disturbances. Section 5 focuses on the structure and the existence in the parameter space of three-dimensional equilibrium solutions emanating from the two-dimensional equilibrium surface. Some conclusions are drawn in §6 with a brief discussion concerning a possible connection between the computed nonlinear states and recent experimental observations.

2. Governing equations and method of solution

We consider an incompressible viscous fluid of viscosity μ^* and constant density ρ^* between two parallel plates located at $y^* = h^*$ and $y^* = -h^*$. The walls are in an uniform parallel motion with wall velocities V^* and $-V^*$ respectively. Introducing a pressure gradient P^*, uniform laminar Poiseuille–Couette flow is defined by the velocity component in the streamwise x^*-direction

$$U^*(y^*) = \frac{-1}{2\mu^*} P^* h^{*2}\left(1-\frac{y^{*2}}{h^{*2}}\right)+\frac{V^*}{h^*}y^*. \tag{2.1}$$

The quantities are non-dimensionalized using the channel half-width h^* and a reference velocity U^* such that in dimensionless form the laminar profile is

$$U(y,\eta) = (1-\eta)(1-y^2)+\eta y. \tag{2.2}$$

For $\eta = 0$ one recovers the parabolic laminar plane Poiseuille flow profile whereas $\eta = 1$ corresponds to the linear plane Couette flow profile. The Reynolds number is $Re = \rho^* U^* h^*/\mu^*$ and the laminar dimensionless pressure gradient $P(\eta) = -2(1-\eta)/Re$ vanishes for the plane Couette flow limit $\eta = 1$ (the reference velocity U^* is then equal to half the velocity difference between the walls V^*). Perturbing the laminar flow we may split the total velocity $\boldsymbol{v}_{tot}$ into two parts

$$\boldsymbol{v}_{tot} = U(y,\eta)\,\boldsymbol{i}+\epsilon\boldsymbol{v}, \tag{2.3}$$

with $\epsilon\boldsymbol{v} = \epsilon(u,v,w)$ the perturbation velocities in the streamwise x-direction, the normal y-direction and the spanwise z-direction respectively. The conveniently chosen

perturbation amplitude ϵ will be fixed by a normalization condition to be specified later. Introducing the disturbance vorticity $\boldsymbol{\omega} = (\xi, \omega, \zeta) = \boldsymbol{\nabla} \times \boldsymbol{v}$ the system can be written in terms of the wall-normal vorticity $\omega = \partial u/\partial z - \partial w/\partial x$ and the wall-normal velocity v as independent variables, the flow geometry being homogeneous in the x-direction and z-direction. In terms of the independent variables the Navier–Stokes system has the form (Ehrenstein & Koch 1991)

$$\frac{\partial}{\partial t}\nabla^2 v = -U\frac{\partial}{\partial x}\nabla^2 v + \frac{\partial^2 U}{\partial y^2}\frac{\partial v}{\partial x} + \frac{1}{Re}\nabla^4 v - \epsilon\left\{\frac{\partial}{\partial x}[(\boldsymbol{v}\cdot\boldsymbol{\nabla})\zeta - (\boldsymbol{\omega}\cdot\boldsymbol{\nabla})w] - \frac{\partial}{\partial z}[(\boldsymbol{v}\cdot\boldsymbol{\nabla})\xi - (\boldsymbol{\omega}\cdot\boldsymbol{\nabla})u]\right\}, \quad (2.4a)$$

$$\frac{\partial}{\partial t}\omega = -Y\frac{\partial \omega}{\partial x} - \frac{\partial U}{\partial y}\frac{\partial v}{\partial z} + \frac{1}{Re}\nabla^2\omega - \epsilon[(\boldsymbol{v}\cdot\boldsymbol{\nabla})\omega - (\boldsymbol{\omega}\cdot\boldsymbol{\nabla})v], \quad (2.4b)$$

together with the boundary conditions

$$v(y = \pm 1) = \frac{\partial v}{\partial y}(y = \pm 1) = 0, \quad (2.4c)$$

$$\omega(y = \pm 1) = 0. \quad (2.4d)$$

In system (2.4) we make use of the continuity equation to get the u- and w-components of the velocity

$$\Delta_1 u = \frac{\partial \omega}{\partial z} - \frac{\partial v}{\partial x\,\partial y}, \quad \Delta_1 w = -\frac{\partial \omega}{\partial x} - \frac{\partial v}{\partial z\,\partial y}, \quad (2.5)$$

with $\Delta_1 = \partial^2/\partial x^2 + \partial^2/\partial z^2$.

The flow geometry being parallel one may assume the solution to be periodic in the streamwise and spanwise directions and the Fourier expansion of the independent variables v, ω is

$$\begin{Bmatrix} v(x, y, z, t) \\ \omega(x, y, z, t) \end{Bmatrix} = \sum_{n=-\infty}^{+\infty} \sum_{m=-\infty}^{+\infty} \begin{Bmatrix} \hat{v}_{nm}(y, t) \\ \hat{\omega}_{nm}(y, t) \end{Bmatrix} \mathrm{e}^{\mathrm{i}n\alpha x + \mathrm{i}m\beta z}. \quad (2.6)$$

Substituting (2.6) into (2.4) using (2.5) together with the definition of the vorticity vector one gets a system of nonlinear modal equations for the Fourier modes $\hat{v}_{nm}, \hat{\omega}_{nm}$ (Ehrenstein & Koch 1991). Reality of the solution requires

$$\hat{v}_{-n,-m} = \bar{\hat{v}}_{n,m}, \quad \hat{\omega}_{-n,-m} = \bar{\hat{\omega}}_{n,m}$$

(where the barred quantities denote the complex conjugate).

Like other investigators (cf. Lundbladh & Johansson 1991) we suppose the disturbance to be symmetric with respect to the plane $z = 0$, in order to reduce the computational effort. Counter-rotating streamwise vortices with similar spanwise symmetries have also been observed during transition in plane Couette flow (cf. Dauchot & Daviaud 1995*b*). Taking into account the symmetry of the solution with respect to $z \to -z$ together with reality of the solution the modal equations have to be solved only for $n \geqslant 0$, $m \geqslant 0$. The system is identically satisfied for $n = m = 0$ and the equation for the disturbance mean flow has to be considered. Averaging the x-momentum equation one gets for the mean flow $\hat{u}_{0,0}(y, t)$

$$\frac{\partial \hat{u}_{0,0}}{\partial t} = \frac{1}{Re}\frac{\mathrm{d}^2 \hat{u}_{0,0}}{\mathrm{d}y^2} - \epsilon[(\boldsymbol{v}\cdot\boldsymbol{\nabla})u]_{0,0} \quad (2.7)$$

(the index $(0,0)$ means that one takes the xz-average). Plane Couette flow is defined by a zero mean pressure gradient and we have used this condition in (2.7). For the numerical computation the modal expansion (2.6) is truncated at $n = N$, $m = M$, and a Chebyshev-collocation method is used to compute the Fourier modes. Each Fourier component is evaluated at $K+1$ collocation points

$$y_j = \cos(j\pi/K), \quad j = 0, 1, \ldots, K, \tag{2.8}$$

and the derivatives are given by the collocation matrix method (cf. Canuto *et al*. 1987).

The purpose of the present work is to compute nonlinear equilibrium states of travelling-wave type which are stationary in a frame of reference moving with the (unknown) wave speed c in the x-direction (steady-state solutions corresponding to $c \equiv 0$). Replacing

$$\frac{\partial}{\partial t} \equiv -c\frac{\partial}{\partial x}$$

in (2.4), (2.7) one readily gets the time-independent set of equations in the corresponding frame of reference. Introducing a stream function ψ by letting

$$-\frac{\partial \psi}{\partial x} = v \quad \text{and} \quad \frac{\partial \psi}{\partial y} = u,$$

a two-dimensional version of the Navier–Stokes system (2.4) can easily be derived in terms of the Fourier expansion of ψ with

$$-\mathrm{i}\alpha n\hat{\psi}_{n0} = \hat{v}_{n0} \quad (\hat{v}_{nm} \equiv 0, \quad m \neq 0; \quad \omega = \xi = w \equiv 0).$$

In order to fix the amplitude ϵ and the phase we use a (quite arbitrary) local normalization condition suitable for both two- and three-dimensional solutions:

$$\hat{\psi}_{10}(0) + \frac{\mathrm{d}\hat{\psi}_{10}(0)}{\mathrm{d}y} = 1. \tag{2.9}$$

Satisfying the modal equations at each collocation point (except the wall boundaries $y = \pm 1$) and adding (2.9) the nonlinear travelling waves are determined by solving a large system of nonlinear algebraic equations:

$$\boldsymbol{F}(\boldsymbol{\lambda}, \boldsymbol{u}) = 0. \tag{2.10}$$

The solution vector $\boldsymbol{u}$ contains the flow quantities as well as the wave speed c and the amplitude ϵ, and $\boldsymbol{\lambda}$ denotes the parameter vector (α, β, Re). The system (2.10) is solved by Newton–Raphson iteration in conjunction with Keller's pseudo-arclength continuation procedure (Keller 1977) in order to avoid the singularities of ordinary parameter continuation at limit points of the solution curve.

3. Two-dimensional nonlinear equilibrium states in plane Couette flow

In this section we summarize results previously published (cf. Cherhabili & Ehrenstein 1995), necessary for the understanding of the subsequent analyses. Due to the lack of primary instability the only way to recover nonlinear states in plane Couette flow is to extend known nonlinear disturbances for a flow geometry somehow connected to plane Couette flow. Here we consider the Poiseuille–Couette flow family, and we apply a continuation procedure to connect nonlinear travelling waves for the pressure-driven plane Poiseuille flow to the plane Couette flow limit. This idea has

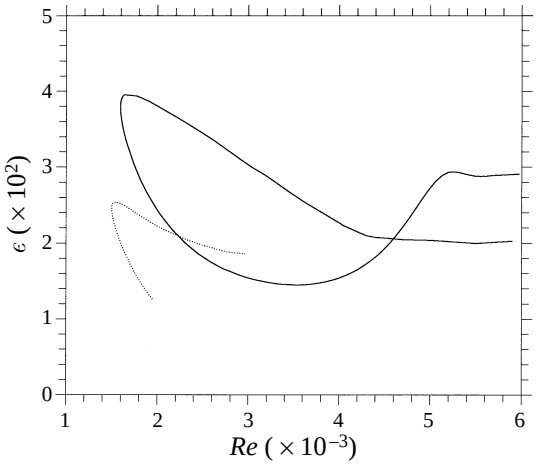

FIGURE 1. Cuts through the two-dimensional equilibrium surface for plane Couette flow in the amplitude ϵ and Reynolds number Re plane for: —, $N = 15, \alpha = 0.17$; $\cdots$, $N = 25, \alpha = 0.10$ ($K = 28$).

previously been advanced by Milinazzo & Saffman (1985) and we first focus on the existence of two-dimensional finite-amplitude states. The nonlinear travelling waves (with $\eta = 0$ in (2.2)) for plane Poiseuille flow bifurcate from the laminar state with a critical propagation speed c determined by linear stability results. The equilibrium surface of this family of non-uniform Poiseuille solutions has been explored in the past (cf. Herbert 1977; Pugh & Saffman 1988).

Increasing progressively the parameter η in (2.2) a thorough exploration of the equilibrium surface in the Poiseuille–Couette parameter space (parameterized by the streamwise wavenumber α and the Reynolds number Re) finally led to the discovery of two-dimensional finite-amplitude states for plane Couette flow with $\eta = 1$ (cf. Cherhabili & Ehrenstein 1995). Surprisingly the nonlinear travelling waves (with $c \neq 0$) for plane Poiseuille flow evolve into stationary ($c = 0$) solitary-like equilibrium states for plane Couette flow. This gives some explanation of why previous attempts to compute two-dimensional finite-amplitude states in plane Couette flow failed.

In what follows the parameter η in (2.2) is that for the plane Couette flow limit ($\eta \equiv 1$) and $c \equiv 0$, the solutions being stationary. A projection of the equilibrium surface on the (ϵ, Re)-plane is shown in figure 1, for two Fourier truncations $N = 15$, 25, the wavenumbers being $\alpha = 0.17$ and 0.10 respectively. For $N = 25$ only the portion of the curve close to the nose has been computed, the limit point being located at $Re \approx 1500$ (which corresponds approximately to the critical Reynolds number for the nonlinear states reported in Cherhabili & Ehrenstein 1995). The streamlines of the corresponding solutions on the upper branches at $Re = 2200$ for both the Fourier truncations are shown in figure 2(a, b). While the periodic boxes (from $x = 0$ and $x = 2\pi/\alpha$) have different lengths the depicted *non-zero* solution structure is almost identical for both the Fourier truncations. To capture these solutions the periodic box with length $\lambda_x = 2\pi/\alpha$ has to be large enough for the solution to be independent of the (periodic) boundary conditions. Also the convergence of these states has to be analysed in terms of Fourier transform rather than Fourier expansion. Interpreting the truncated Fourier expansion as a discrete Fourier transform (in x) the following relationship between the Fourier transform $\boldsymbol{\phi}$ of the disturbance and the (normalized) Fourier modes $\boldsymbol{v}_n(y)$ holds:

$$\boldsymbol{\phi}(\alpha n, y) = (2\pi/\alpha)\,\epsilon \boldsymbol{v}_n(y), \quad 0 \leqslant n \leqslant N. \tag{3.1}$$

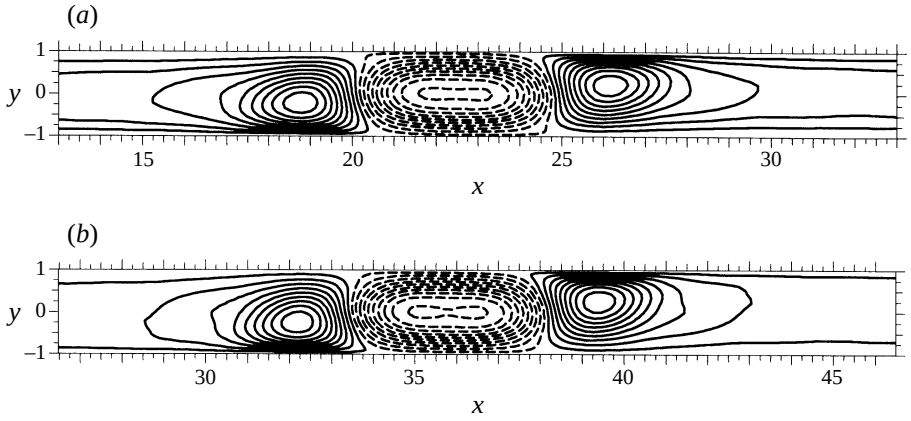

FIGURE 2. Streamlines of the spatially localized two-dimensional disturbance for plane Couette flow at $Re = 2200$: (*a*) $N = 15$; (*b*) $N = 25$ ($K = 28$).

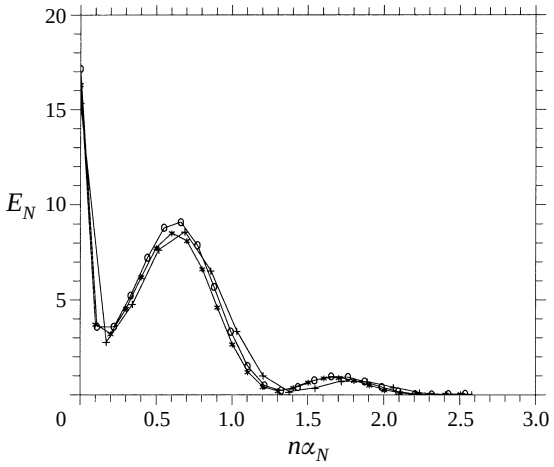

FIGURE 3. Energy E_N of the streamwise Fourier transform for two-dimensional equilibrium states at $Re = 2200$, with $N\alpha_N \approx$ constant. +, $N = 15$, $\alpha_{15} = 0.172$; ○, $N = 23$, $\alpha_{23} = 0.1103$; ∗, $N = 25$, $\alpha_{25} = 0.10$ ($K = 28$).

Hence the ratio ϵ/α is more appropriate to characterize the solution than the amplitude ϵ alone and, comparing the curves of figure 1 at the nose for both the N-values, ϵ/α is close to 0.25. The Fourier transform of a localized structure being zero outside a closed interval, the wavenumber α_N depends on the Fourier truncation N through $\alpha_N N =$ constant. Fully converged spatially localized nonlinear states are ultimately obtained for decreasing wavenumber α with increasing Fourier truncation N, which can be interpreted as a homoclinic bifurcation of a limit-cycle solution in a phase-space formulation of the flow (cf. Pumir, Manneville & Pomeau 1983). Figure 3 depicts the integral quantity

$$E_N(\alpha_N n) = \int_{-1}^{1} |\boldsymbol{v}_n(y)|^2 \,\mathrm{d}y, \quad 0 \leqslant n \leqslant N, \tag{3.2}$$

for different values of N with $\alpha_N N \approx 2.5$ ($Re = 2200$). The Fourier transforms for the

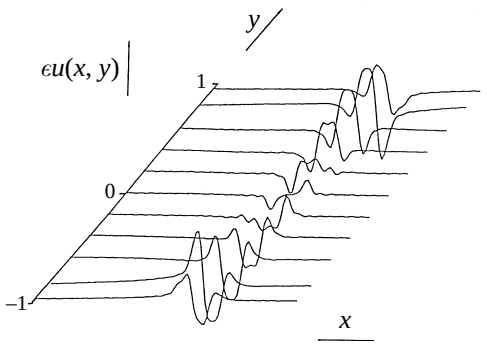

FIGURE 4. Perspective view over one wavelength in x and across the channel y of the streamwise component ϵu of the two-dimensional nonlinear disturbance in plane Couette flow, at $Re = 2200$, with $N = 25$, $\alpha = 0.11$ ($K = 28$).

three truncations $N = 15$, 23, 25 almost coincide, hence $N = 15$ should provide fairly converged solutions. Finally figure 4 depicts the structure of the streamwise component of the nonlinear equilibrium state. This solution at $Re = 2200$ (located on the upper branch of the corresponding cut through the equilibrium surface) has been computed with a Fourier truncation $N = 25$ and with 29 collocation points ($K = 28$ in (2.8)). The spatially localized state is symmetric with respect to the centre of the structure. The amplitude of the solution increases when approaching the walls at $y = \pm 1$ (before being zero due to the no-slip condition for the disturbance). The $y =$ constant cuts consist of two-hump profiles at mid-channel and three-hump profiles close to the walls.

As for other shear flows (cf. Herbert 1988) secondary instabilities are expected to play an important role in the transition process. Therefore the next step will be to analyse the stability of the two-dimensional states with respect to secondary disturbances.

4. Stability of the two-dimensional equilibrium states

The Navier–Stokes system (2.4) can formally be written as a (infinite-dimensional) dynamical system

$$\frac{\partial}{\partial t}\boldsymbol{\phi} = \mathrm{L}(U, Re)\,\boldsymbol{\phi} + \mathcal{N}\mathcal{L}(\boldsymbol{\phi}) \tag{4.1}$$

for $\boldsymbol{\phi} = (v, \omega)$. Here $\mathrm{L}(U, Re)$ stands for the linear operator depending on the laminar plane Couette flow profile $U(y)$ and the Reynolds number Re, the nonlinear advection terms are written as $\mathcal{N}\mathcal{L}(\boldsymbol{\phi})$. (Here we implicitly assume that the operator ∇^2 on the left-hand side of (2.4a) has been inverted.) The nonlinear time-independent solutions discussed in the previous section are equilibrium states of (4.1), that is

$$\mathrm{L}(U, Re)\,\boldsymbol{\phi}_{2D} + \mathcal{N}\mathcal{L}(\boldsymbol{\phi}_{2D}) = 0, \quad \text{with} \quad \boldsymbol{\phi}_{2D} = (v_{2D}, 0).$$

Superimposing a perturbation

$$\boldsymbol{\phi}_{2D} + \tau\boldsymbol{\psi}\mathrm{e}^{\sigma t}$$

one obtains by linearizing the right-hand side of (4.1)

$$\sigma\boldsymbol{\psi} = \mathcal{J}(U, Re, \boldsymbol{\phi}_{2D})\,\boldsymbol{\psi}, \tag{4.2a}$$

where $$\mathscr{J}(U, Re, \boldsymbol{\phi}_{2D})\,\boldsymbol{\psi} = \mathrm{L}(U, Re)\,\boldsymbol{\psi} + \frac{\partial}{\partial \tau}(\mathscr{N}\mathscr{L}(\boldsymbol{\phi}_{2D} + \tau\boldsymbol{\psi}))|_{\tau=0}. \tag{4.2b}$$

The two-dimensional equilibrium state is given as a Fourier expansion

$$v_{2D}(x, y) = \sum_{n=-N}^{N} \hat{v}_n(y)\,\mathrm{e}^{\mathrm{i}n\alpha x}$$

(the modes $\hat{v}_n(y)$ being discretized using Chebyshev-collocation). Hence by Floquet theory (cf. Herbert 1988) and introducing a spanwise wavenumber β we are seeking a (three-dimensional) secondary eigensolution $\boldsymbol{\psi}$ of the form

$$\boldsymbol{\psi} = \begin{Bmatrix} v \\ \omega \end{Bmatrix} = \begin{Bmatrix} \sum_{n=-N}^{N} \hat{v}_{n1}(y)\,\mathrm{e}^{\mathrm{i}n\alpha x} \\ \sum_{n=-N}^{N} \hat{\omega}_{n1}(y)\,\mathrm{e}^{\mathrm{i}n\alpha x} \end{Bmatrix} \mathrm{e}^{\mathrm{i}\beta z}. \tag{4.3}$$

The operator in (4.2), the problem once discretized, is identical to the Jacobian matrix of the nonlinear system (2.10) evaluated at the two-dimensional nonlinear state. Hence the stability is analysed solving a large matrix-eigenvalue problem with eigenvalue σ, the two-dimensional nonlinear state being unstable if the real part $\mathrm{Re}\,(\sigma) > 0$. Two-dimensional perturbations are such that $\omega \equiv 0$ and $\beta = 0$ in (4.3).

Note that for a general secondary stability analysis of two-dimensional nonlinear waves one should multiply (4.3) by a factor $\mathrm{e}^{\mathrm{i}\gamma x}$, $0 \leqslant \gamma < \alpha$ (cf. Herbert 1988). However, for plane Poiseuille flow (Ehrenstein & Koch 1991) or the Blasius boundary layer (Koch 1992; Ehrenstein & Koch 1995) phase-locked superharmonic disturbances (with $\gamma \equiv 0$) play a major role in the subcritical transition process. In the present case the two-dimensional (stationary) nonlinear states are localized in the streamwise direction rather than periodic. Here we focus in our temporal stability analysis on disturbances using the same periodic box in the streamwise direction as the nonlinear steady state (which already necessitates considerable computational efforts).

The matrix-eigenvalue problem for two-dimensional disturbances is solved using a standard eigenvalue routine. Owing to the system size for the secondary three-dimensional stability analysis we also used Arnoldi-type algorithms together with a shift-and-invert strategy suitable for the computation of the most unstable part of the eigenvalue spectrum (cf. Nayar & Ortega 1993).

4.1. *Two-dimensional secondary instabilities*

Superimposing two-dimensional disturbances on the nonlinear equilibrium states, the limit points in the Reynolds number (for a fixed streamwise wavenumber α) of the equilibrium surface (cf. figure 1) are bifurcation points where a real eigenvalue (corresponding to a secondary two-dimensional eigenmode) crosses zero. Figure 5 depicts stability computations in the vicinity of the limit points for both the wavenumbers $\alpha = 0.111$ and 0.175. The real parts of the most unstable eigenvalues for the solutions on the upper and the lower branches of the corresponding cuts through the equilibrium surface are shown. The most unstable eigenvalues on the upper branch for $\alpha = 0.111$ are depicted as crosses and at the limit point (at $Re \approx 2150$) a second real eigenvalue (marked as small circles) crosses zero. Both real eigenvalues collide in the vicinity of the limit point and a complex eigenvalue with increasing non-zero imaginary part appears along the lower branch of the cut through the equilibrium surface. While

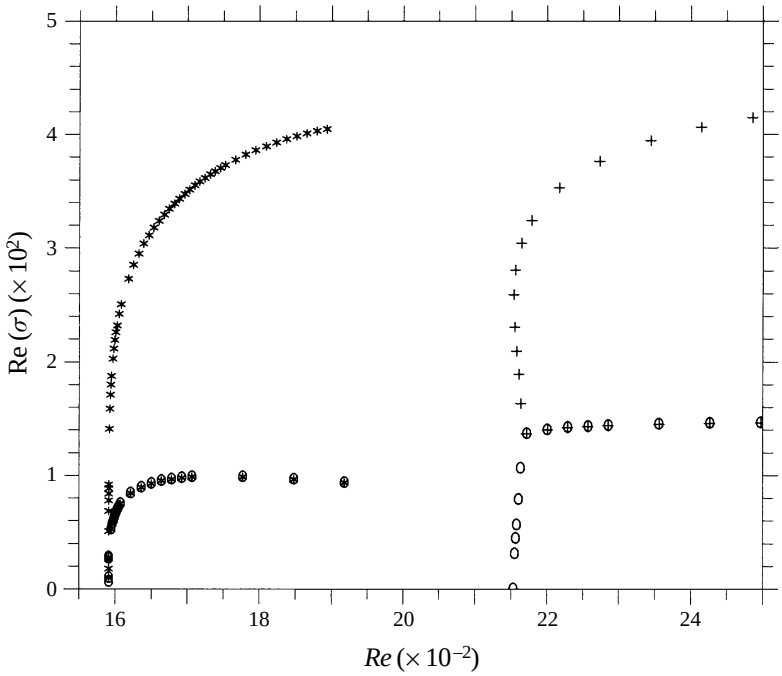

FIGURE 5. Highest two-dimensional secondary amplification rates $\mathrm{Re}(\sigma)$ as a function of Re, $N = 15$ ($K = 28$). Computations for $\alpha = 0.111$: $+$, $\mathrm{Im}(\sigma) = 0$, (upper branch); $\bigcirc$, $\mathrm{Im}(\sigma) = 0$; $\oplus$, $\mathrm{Im}(\sigma) \neq 0$ (lower branch). Computations for $\alpha = 0.175$: $*$, $\mathrm{Im}(\sigma) = 0$ (upper branch); $\otimes$, $\mathrm{Im}(\sigma) \neq 0$ (lower branch).

for the wavenumber $\alpha = 0.111$ the real eigenvalues collide in the unstable region $\mathrm{Re}(\sigma) > 0$, the collision occurs very close to the neutral line $\mathrm{Re}(\sigma) = 0$ for a fixed wavenumber $\alpha = 0.175$ (the unstable real eigenvalues on the upper branch are depicted as stars in figure 5). This can be explained as follows. For the wavenumber $\alpha = 0.175$ the limit point at $Re \approx 1580$ is close to the lowest Reynolds number for the existence of the two-dimensional nonlinear equilibrium states (computed with Fourier truncation $N = 15$ and $K = 28$). Hence the limit point is close to a double-limit point in the Reynolds number Re and the wavenumber α, where the linearized equation (4.2) has a zero eigenvalue with algebraic multiplicity two and geometric multiplicity one. As can be shown by local analyses (cf. Guckenheimer & Holmes 1983) those double-zero bifurcations are responsible for the emergence of complex-conjugate eigenvalues.

Double-zero bifurcations have also been observed on the two-dimensional equilibrium surface in plane Poiseuille flow (cf. Pugh & Saffman 1988; Soibelman & Meiron 1991). Introducing in addition to the Reynolds number a second parameter which parameterizes the plane Poiseuille flow problem relative to a constant-flux formulation or a constant-pressure-gradient formulation Barkley (1990) interpreted the occurrence of the complex eigenvalue (a Hopf bifurcation) in terms of dynamical systems theory. In the present plane Couette flow case, the second parameter is the wavenumber α and the collision between the real eigenvalues at the nose of the equilibrium surface can be interpreted as a degenerate Hopf bifurcation. Indeed for wavenumbers in the vicinity of the critical value $\alpha_c \approx 0.175$ (with $N = 15$) the real eigenvalues always collide in the unstable region $\mathrm{Re}(\sigma) > 0$ (in figure 5 we have only shown the results for a wavenumber $\alpha < \alpha_c$).

In summary the stability computations for two-dimensional secondary perturbations

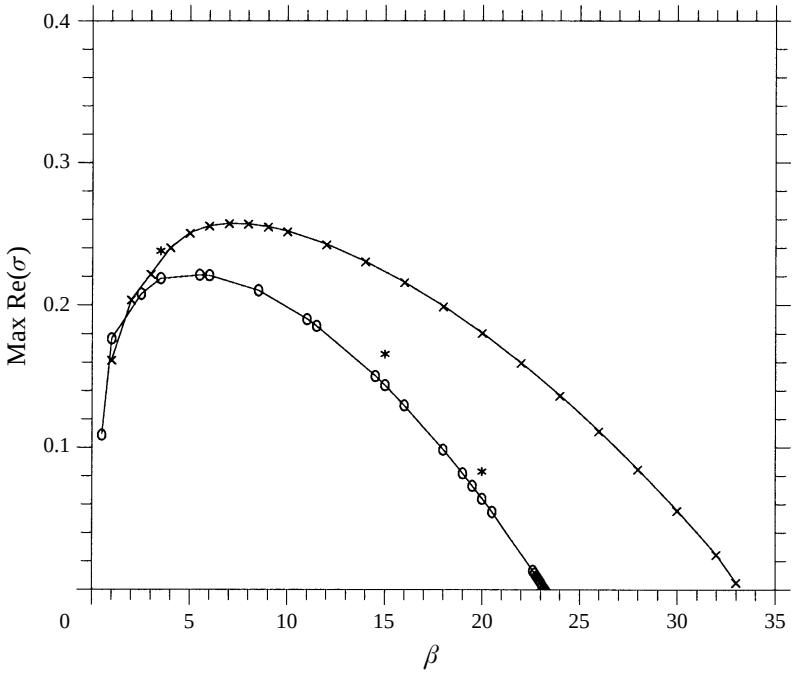

FIGURE 6. Highest three-dimensional secondary amplification rates $\mathrm{Max}\,\mathrm{Re}(\sigma)$ as a function of spanwise wavenumber β. ○, Mode with $\mathrm{Im}(\sigma) = 0$, $Re = 2200$, $N = 13$ ($\alpha = 0.132$); ∗, Mode with $\mathrm{Im}(\sigma) = 0$, $Re = 2200$, $N = 15$ ($\alpha = 0.111$); ×, Mode with $\mathrm{Im}(\sigma) = 0$, $Re = 4000$, $N = 13$ ($\alpha = 0.132$).

show that (for a fixed wavenumber α) the upper branches of the two-dimensional equilibrium surfaces are unstable with respect to steady ($\mathrm{Im}(\sigma) = 0$) secondary two-dimensional instabilities whereas the lower branches are unstable to oscillatory disturbances. In plane Poiseuille flow (Soibelman & Meiron 1991) oscillatory two-dimensional instabilities have been observed on the upper branches of the two-dimensional equilibrium surface rather than the lower branches. Inspecting figure 1 the lower branch for the Reynolds number region $Re < 4500$ corresponds in fact to the upper branch with almost constant amplitude ϵ for higher Reynolds numbers. The branches cross each other in the projection on the (ϵ, Re)-plane at $Re \approx 4600$.

4.2. *Three-dimensional secondary instability*

The dynamics during transition in shear flows is certainly dominated by three-dimensional secondary instabilities. Taking into account three-dimensional perturbations (4.3) a new parameter appears via the spanwise wavenumber β. Linearizing the Navier–Stokes equations at two-dimensional equilibrium states located on the lower branch of the equilibrium surface, highest amplification rates $\mathrm{Re}(\sigma)$ for three-dimensional perturbations as a function of β are depicted in figure 6, for fixed Reynolds numbers $Re = 2200$ and 4000 (with wavenumber $\alpha = 0.132$). A streamwise Fourier truncation of $N = 13$ has been used to compute the two-dimensional states (with 29 Chebyshev polynomials in the wall-normal direction) leading to a matrix eigenvalue problem of almost 2200 real equations. The most unstable eigenvalues shown in figure 6 are real. For $Re = 2200$ the maximum amplification is reached at $\beta \approx 5$ and $\mathrm{Re}(\sigma)$ decreases for increasing β before crossing the line $\mathrm{Re}(\sigma) = 0$ at $\beta_c \approx 23$, defining a cut-off spanwise wavelength $\lambda_z = 2\pi/\beta_c$. The behaviour is similar for the computations at $Re = 4000$ (cf. figure 6), the critical spanwise wavenumber now being located at

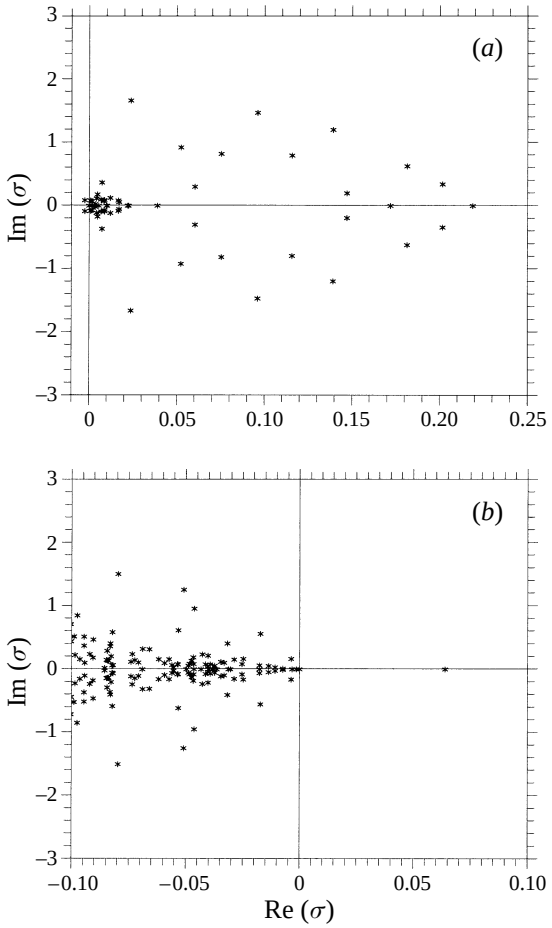

FIGURE 7. Principal part of the three-dimensional secondary eigenvalue spectrum for the solution on the two-dimensional equilibrium surface at $Re = 2200$, with $\alpha = 0.132$, $N = 13$ ($K = 28$). (*a*) $\beta = 3.5$; (*b*) $\beta = 20$.

$\beta_c \approx 33$. The truncation $N = 13$ is a lower limit for the two-dimensional solutions to be reasonably converged (cf. Cherhabili & Ehrenstein 1995) and we performed some stability computations with $N = 15$ (at $Re = 2200$ with $\alpha = 0.11$) marked as stars in figure 6. Beside a small shift in the amplification rate the results fit reasonably well with the results for the lower truncation $N = 13$. Figure 7(*a*, *b*) depicts the principal part of the stability spectrum (for the two-dimensional equilibrium state at $Re = 2200$) for three-dimensional perturbations for two different spanwise wavenumbers β. While for $\beta = 3.5$ complex and real eigenvalues are unstable besides the most unstable real one, for $\beta = 20$ only one unstable eigenvalue is left.

Inspecting figure 6, one observes that the highest amplification rates for three-dimensional perturbations (at $\beta \approx 5$) are almost an order of magnitude higher than the amplification rates for two-dimensional perturbations depicted in figure 5. Contrary to plane Poiseuille flow where oscillatory secondary instabilities dominate for large β-values (cf. Ehrenstein & Koch 1991), for the present plane Couette flow computations the critical spanwise wavenumbers β_c are parameters for steady bifurcations to three-dimensional equilibrium solutions (beside the weak oscillatory instability due to two-dimensional secondary eigenmodes).

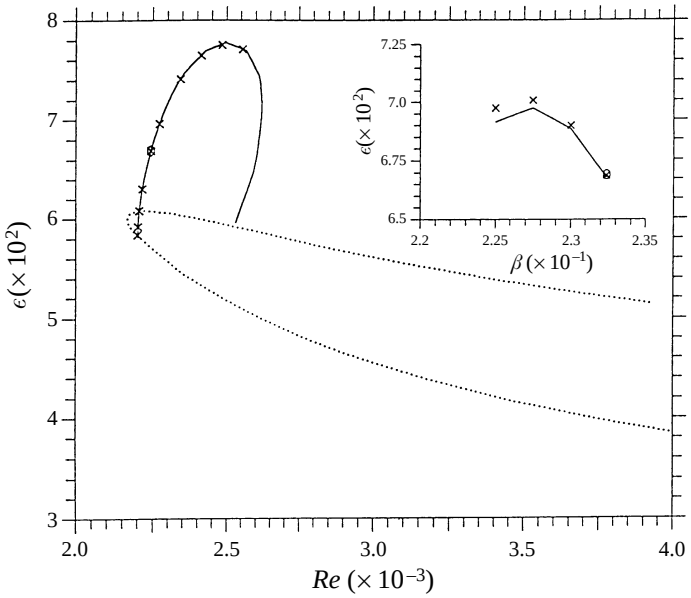

FIGURE 8. Cut through the equilibrium surface in the amplitude ϵ and Reynolds number Re plane: $\cdots$, two-dimensional equilibrium state for $N = 13$, $\alpha = 0.132$ ($K = 28$); —, bifurcating three-dimensional branch for spanwise wavenumber $\beta_c = 23.2406$ with $M = 1$ ($\alpha = 0.132$, $N = 13$); $\times$, three-dimensional solutions for $\beta_c = 23.2406$ with $M = 2$ ($\alpha = 0.132$, $N = 13$). The insert shows a cut through the equilibrium surface in the (ϵ,β)-plane, at $Re = 2250$, for β in the vicinity of β_c: —, $M = 1$, $\times$, $M = 2$.

5. Three-dimensional nonlinear equilibrium states

Starting with the neutrally stable secondary eigensolutions on the two-dimensional nonlinear equilibrium surface, bifurcating nonlinear three-dimensional equilibrium states can be computed solving the complete *three-dimensional stationary* Navier–Stokes equations following the solution procedure outlined in §2. We use the spanwise symmetry assumption hence the three-dimensional branches emerge as pitchfork bifurcations similar to the plane Poiseuille flow analysis (Ehrenstein & Koch 1991; Ehrenstein 1994). To capture the solution branches it was necessary to compute the critical spanwise wavenumbers β_c with a high accuracy in order to isolate the corresponding eigensolution necessary for the branch capturing procedure (cf. Keller 1977). Locating the critical spanwise wavenumber at $\beta_c = 23.2406$ (cf. figure 6) for the equilibrium state at $Re = 2200$ (with $N = 13$ and $\alpha = 0.132$) the three-dimensional equilibrium solutions are shown as the solid line on figure 8. The cut through the two-dimensional equilibrium surface is represented as the dashed line and the family of three-dimensional solutions connects the lower and the upper branch. The solutions corresponding to the solid line have been computed with the spanwise Fourier truncation $M = 1$ in (2.6) and some solutions with $M = 2$ are also shown marked as crosses in the (ϵ, Re)-plane. The results for both the truncations coincide, at least for that small spanwise cut-off wavelength $\lambda_z = 2\pi/\beta_c$. Starting from the solution marked as an encircled cross, the insert of figure 8 shows some three-dimensional equilibrium states in the (ϵ, β)-plane in the vicinity of β_c (for a fixed Reynolds number $Re = 2250$). While the solutions for both the truncations $M = 1$, $M = 2$ coincide at β_c, they diverge for decreasing β. The nonlinear system with $N = 13$ and $M = 2$ ($K = 28$) consists of almost 3650 real equations and this is at the very limit of the capacity of our

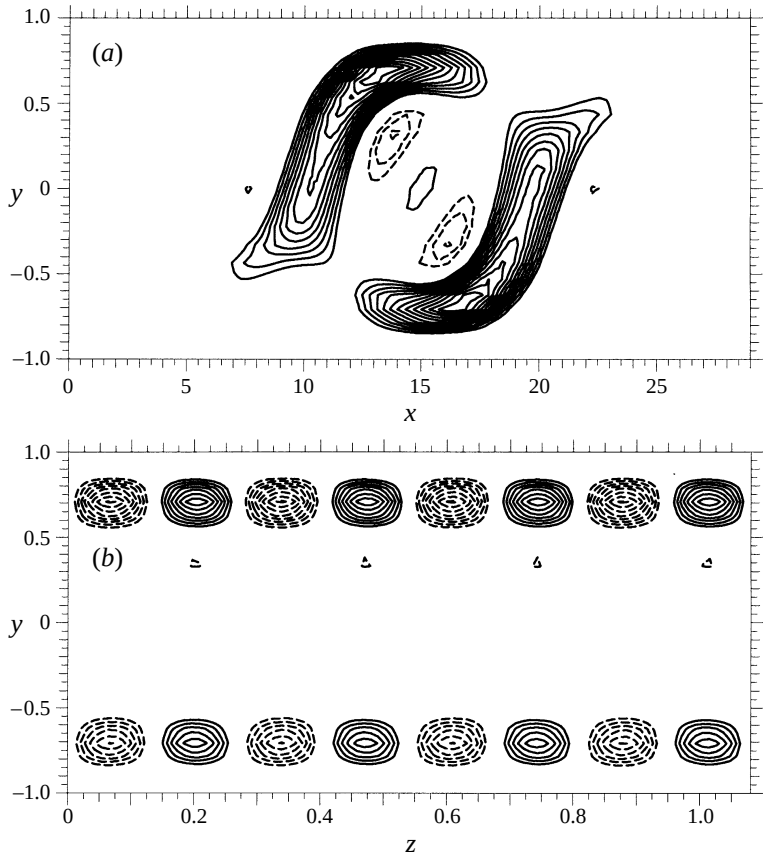

FIGURE 9. Lines of constant streamwise vorticity for the three-dimensional equilibrium state marked $\otimes$ on figure 8, at $Re = 2243$ ($\alpha = 0.132$, $\beta = 23.2406$). (*a*) Lines in the plane $z = 1$. (*b*) Lines in the plane $x = 14.5$, over four wavelengths in z.

computational facilities. (The computations have been performed on the IBM/SP2 of the CNUSC, France, as well as on a 128 Mbyte workstation digital alphastation 200 4/166. One iteration in the Newton–Raphson solution procedure necessitates about 70 minutes CPU on the workstation, convergence being achieved within five iterations, except near limit points where up to eight iterations are necessary.)

The spatial structure of the three-dimensional equilibrium state is shown in figures 9 and 10 (the corresponding solution is marked as the encircled cross in figure 8). In figure 9 the streamwise vorticity is depicted: the isolines in the (x, y)-plane (for fixed $z = 1$) are shown in figure 9(*a*) whereas figure 9(*b*) depicts isolines in the (y, z)-plane. The $x =$ constant cut shown in figure 9(*b*) has been performed at $x = 14.5$, close to the centre of the non-zero structure where the vorticity is maximal. Whereas the solution is localized in the streamwise direction it exhibits pairs of counter-rotating patterns near the walls in the (y, z)-plane. The non-zero solution structure in figure 9(*a*) extends from $x \approx 6$ to 23 inside the streamwise-periodic box (from $x = 0$ to $x = 2\pi/\alpha \approx 48$). Hence the streamwise width of the solution is about eight times the channel height. The normal vorticity ω is depicted in figure 10. Figure 10(*a*) shows the isolines in the (x, y) plane (for $z = 1$). The counter-rotating structure at mid-channel $y = 0$ (with a finite width in the streamwise direction) is depicted in figure 10(*b*).

It would be impossible to perform an exhaustive exploration of the three-

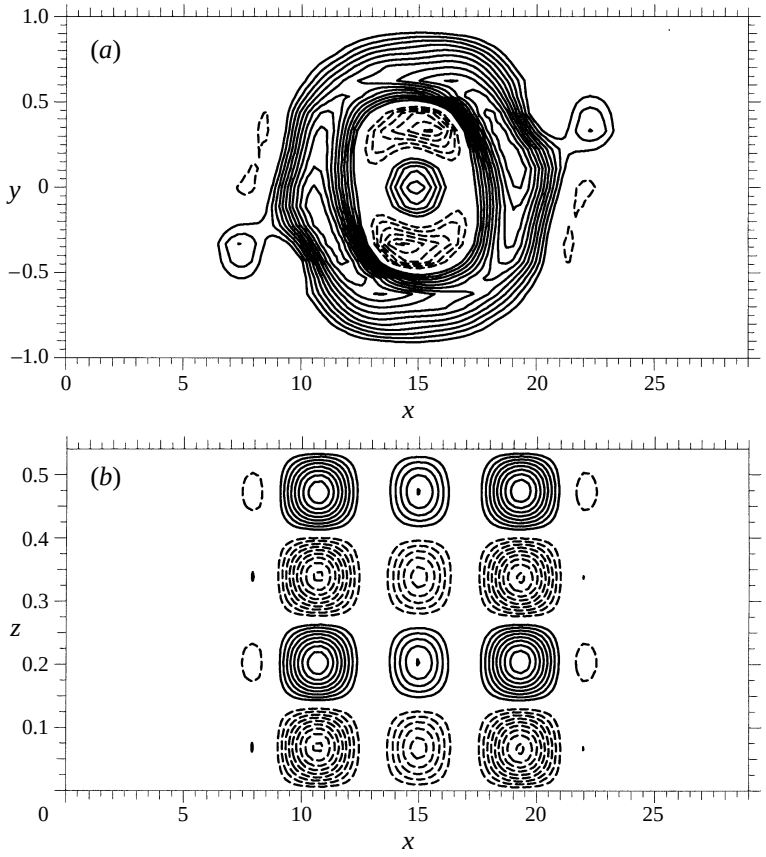

FIGURE 10. Lines of constant normal vorticity, same solution as figure 9. (*a*) Lines in the plane $z = 1$. (*b*) Lines in the plane $y = 0$, over two wavelengths in z.

dimensional equilibrium surface. Therefore, we have to focus on a strategy in order to reach Reynolds numbers below the limit point of the two-dimensional equilibrium surface. In plane Poiseuille flow (Ehrenstein & Koch 1991) or in the Blasius boundary-layer flow (Ehrenstein & Koch 1995) three-dimensional equilibrium states containing only even spanwise Fourier modes appeared to be of particular importance for a subcritical bifurcation analysis. Performing a stability analysis truncating at $M = 2$ in (2.6), the first spanwise harmonic (i.e. $m = 2$) is neutrally stable at $\beta_c/2$ where β_c is the critical spanwise wavenumber for the fundamental mode $m = 1$. For instance for the stability results (at $Re = 2200$) depicted in figure 6 the branch containing only even spanwise Fourier modes bifurcates at approximately $\beta_c/2 \approx 11.5$.

We started at this bifurcation point, marked as a point on the cut through the two-dimensional equilibrium surface in figure 11, and we decreased the spanwise wavenumber β in the hope of finding three-dimensional equilibrium solutions in the lower-Reynolds-number region. In figure 11 some results are depicted in the (ϵ, Re)-plane, the different symbols represent three-dimensional solutions for decreasing spanwise wavenumbers β leading to lower Reynolds numbers. The computations were very time consuming (in particular it was necessary to use very small parameter variations in the continuation procedure) and the last point reached, marked as an encircled cross, is located at $Re \approx 1100$. For this Reynolds number region close to 1000, almost eight iterations were necessary for convergence with vanishing parameter

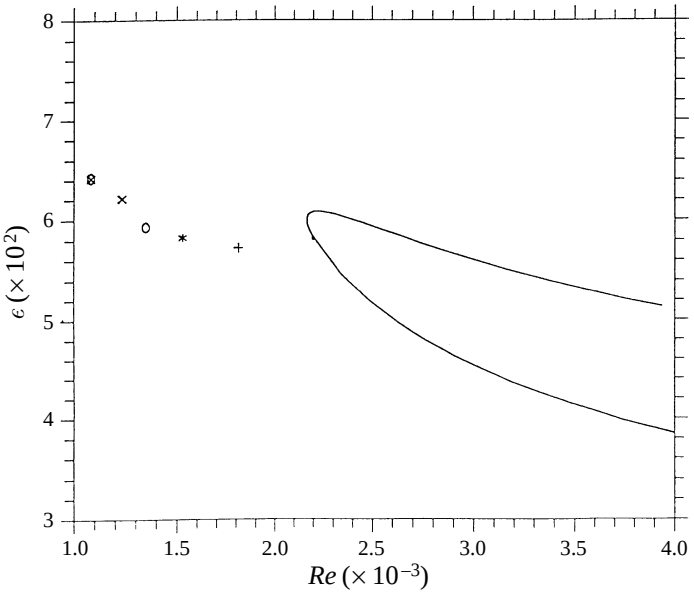

FIGURE 11. Cut through the equilibrium surface in the amplitude ϵ and Reynolds number Re plane: —, two-dimensional equilibrium state for $N = 13$, $\alpha = 0.132$ ($K = 28$). The discrete points correspond to three-dimensional equilibrium states with only even spanwise Fourier modes, $M = 2$: $\cdot$, $\beta = 11.62$; $+$, $\beta = 10.25$; $*$, $\beta = 9.75$; $\bigcirc$, $\beta = 8.85$; $\times$, $\beta = 8.4$; $\otimes$, $\beta = 7.6$.

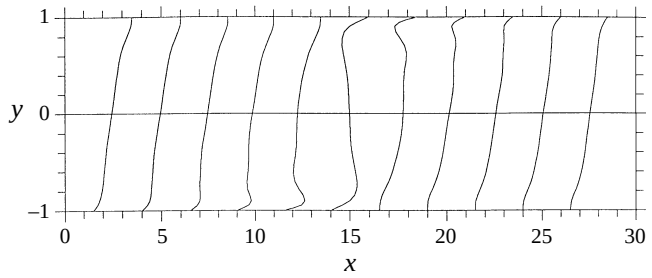

FIGURE 12. Plane Couette flow spanwise-averaged streamwise velocity profiles for the solution at $Re = 1100$, with $\beta = 7.6$, $\alpha = 0.132$, $N = 13$, $M = 2$ ($K = 28$), within the perturbed region in x. The intersection of the profiles with the abscissa corresponds to the x-location of the respective profile, with $\Delta u = \Delta x$. The solution is marked $\otimes$ on figure 11.

variations. While this last point does not represent the overall limit point of the equilibrium surface for three-dimensional solutions it is below the Reynolds number region of the two-dimensional equilibrium surface. One may hypothesize that a higher resolution is necessary to extend the equilibrium surface. In particular the streamwise truncation of $N = 13$ (with $\alpha = 0.132$) is already a lower limit for reasonably converged two-dimensional solutions (Cherhabili & Ehrenstein 1995). We again emphasize that the solutions have been computed solving system (2.10) with about 3650 nonlinear equations and it would hardly be possible to increase the spatial resolution.

In figure 12 profiles of the spanwise-averaged streamwise velocity component are shown, the corresponding three-dimensional solution at $Re = 1100$ is marked as the encircled cross in figure 11. The profile at $x \approx 15$ exhibits the typical S-shaped structure of spatially filtered profiles in transitional or turbulent plane Couette flow (Lundbladh & Johansson 1991). On both sides of the central S-shaped profile the velocity profiles,

which are symmetric with respect to the centre located at $x \approx 15$ and $y = 0$, evolve into the linear laminar Couette profile. This again illustrates the presence of a spatially localized perturbed state.

6. Conclusions

A numerical bifurcation study for plane Couette flow has been performed by computing successive equilibrium states, solutions of the Navier–Stokes equations. To circumvent the lack of critical parameter values in plane Couette flow, first nonlinear states have been computed which are connected parameterically to plane Poiseuille flow through the Poiseuille–Couette flow family. This procedure led to the discovery of two-dimensional stationary nonlinear states in plane Couette flow spatially localized in the streamwise direction. These new solutions are subject to secondary instabilities with respect to two-dimensional and three-dimensional disturbances. As expected and similar to other shear flows three-dimensional disturbances dominate in the neighbourhood of the two-dimensional equilibrium surface. The most strongly growing disturbances have eigenvalues with zero imaginary part and cut-off spanwise wavelengths have been computed for the emergence of three-dimensional stationary equilibrium states. These solutions are periodic in the spanwise direction and spatially localized in the streamwise direction. The complex spatial structure of these solutions necessitates a high resolution and the nonlinear states could be located for Reynolds numbers close to 1000. Even though secondary bifurcation sequences are similar for plane Couette flow and plane Poiseuille flow, the localized streamwise structure makes the nonlinear plane Couette flow states a qualitatively different solution. The present computations may provide some explanation for the difficulties one encounters in computing reliable statistics in turbulent plane Couette flow. Indeed Bech *et al.* (1995) report that those computations are strongly dependent on the size of the periodic streamwise box.

Experiments in plane Couette flow revealed the stable coexistence of laminar and turbulent domains (Tillmark & Alfredsson 1991; Daviaud *et al.* 1992). Coherent structures spatially localized in the streamwise direction and with a counter-rotating structure in the spanwise direction have recently been identified experimentally in plane Couette flow (Dauchot & Daviaud 1995*b*). While there are possible connections between our findings and observed flow structures, we did not succeed in computing nonlinear states for such low Reynolds numbers as reported in the experiments. One may hypothesize that by increasing the numerical resolution (beyond the capability of our computational facilities) one could reach lower Reynolds number regions.

The successive nonlinear states being (stationary) equilibrium solutions, plane Couette flow is not only a prototype of a shear flow with a subcritical transition behaviour but also a case study with regard to the interpretation of the Navier–Stokes system as a dynamical system. The results reported in the present work reinforce the hypothesis that subcritical transition is related to the existence of nonlinear equilibrium states which are (in general unstable) fixed points of the Navier–Stokes equations (cf. Waleffe 1995; Dauchot & Manneville 1997).

Computations of three-dimensional equilibrium states in plane Couette flow have also been reported by Nagata (1990) as a limit case in a Taylor–Couette system and by Busse & Clever (1996) for vanishing Rayleigh number in a Bénard–Couette system. Unlike our findings the solutions reported by Nagata and Busse & Clever do not exhibit a localized structure in the streamwise direction. One may hypothesize that different procedures used to connect flow configurations parameterically to plane Couette flow may lead to different solution classes.

We are grateful to Olivier Dauchot and François Daviaud for stimulating discussions concerning a possible connection between our computations and their experimental findings. Parts of the computations have been performed on the IBM/SP2 of the CNUSC, France.

REFERENCES

Andersson, H. I., Bech, K. H. & Kristoffersen, R. 1992 On diffusion of turbulent energy in plane Couette flow. *Proc. R. Soc. Lond.* A **438**, 477–484.

Aydin, E. M. & Leutheusser, H. J. 1991 Plane–Couette flow between smooth and rough walls. *Exps Fluids* **11**, 302–312.

Baggett, J. S., Driscoll, T. A. & Trefethen, L. N. 1995 A mostly linear model of transition to turbulence. *Phys. Fluids* **7**, 833–838.

Barkley, D. 1990 Theory and prediction for finite-amplitude waves in two-dimensional plane Poiseuille flow. *Phys. Fluids* A **2**, 955–969.

Bech, K. H., Tillmark, N., Alfredsson, P. H. & Andersson, H. I. 1995 An investigation of turbulent plane Couette flow at low Reynolds numbers. *J. Fluid Mech.* **286**, 291–325.

Busse, F. H. & Clever, R. M. 1996 Bifurcation sequences in problems of thermal convection and of plane Couette flow. In *Waves and Nonlinear Processes in Hydrodynamics* (ed. J. Grue *et al.*), pp. 209–226. Kluwer.

Canuto, C., Hussaini, A., Quarteroni, A. & Zang, T. A. 1987 *Spectral Methods in Fluid Dynamics*. Springer.

Cherhabili, A. & Ehrenstein, U. 1995 Spatially localized two-dimensional finite-amplitude states in plane Couette flow. *Eur. J. Mech.* B/*Fluids* **14**, 677–696.

Clever, R. M. & Busse, F. H. 1992 Three-dimensional convection in a horizontal fluid layer subjected to a constant shear. *J. Fluid Mech.* **234**, 511–527.

Cowley, S. J. & Smith, F. T. 1985 On the stability of Poiseuille–Couette flow: a bifurcation from infinity. *J. Fluid Mech.* **156**, 83–100.

Dauchot, O. & Daviaud, F. 1995*a* Finite-amplitude perturbation and spot growth mechanism in plane Couette flow. *Phys. Fluids* **7**, 335–343.

Dauchot, O. & Daviaud, F. 1995*b* Streamwise vortices in plane Couette flow. *Phys. Fluids* **7**, 901–903.

Dauchot, O. & Manneville, P. 1997 Local *versus* global concepts in hydrodynamic stability theory. *J. Phys.* II *Paris* **7**, 371–389.

Daviaud, F., Hegseth, J. & Bergé, P. 1992 Subcritical transition to turbulence in plane Couette flow. *Phys. Rev. Lett.* **69**, 2511–2514.

Dubrulle, B. & Zahn, J. P. 1991 Nonlinear instability of viscous plane Couette flow. Part 1. Analytical approach to a necessary condition. *J. Fluid Mech.* **231**, 561–573.

Ehrenstein, U. 1994 Secondary bifurcations in plane Poiseuille flow with three interacting modes. *Phys. Lett.* A **186**, 403–409.

Ehrenstein, U. & Koch, W. 1991 Three-dimensional wavelike equilibrium states in plane Poiseuille flow. *J. Fluid Mech.* **228**, 111–148.

Ehrenstein, U. & Koch, W. 1995 Homoclinic bifurcation in Blasius boundary-layer flow. *Phys. Fluids* **7**, 1282–1291.

Guckenheimer & Holmes 1983 *Nonlinear Oscillations Dynamical systems and Bifurcations of Vector Fields*. Springer.

Herbert, T. 1977 Die Neutralfläche der ebenen Poiseuilleströmung. Habilitationsschrift, Universität Stuttgart.

Herbert, T. 1988 Secondary instability of boundary layers. *Ann. Rev. Fluid Mech.* **20**, 487–526.

Keller, H. B. 1977 Numerical solution of bifurcation and nonlinear eigenvalue problems. In *Application of Bifurcation Theory* (ed. P. H. Rabinowitz), pp. 359–384. Academic.

Koch, W. 1992 On a degeneracy of temporal secondary instability modes in Blasius boundary-layer flow. *J. Fluid Mech.* **243**, 319–351.

Kreiss, G., Lundbladh, A. & Henningson, D. S. 1994 Bounds for threshold amplitudes in subcritical shear flows. *J. Fluid Mech.* **270**, 175–198.

Lerner, J. & Knobloch, E. 1988 The long-wave instability of a defect in a uniform parallel shear. *J. Fluid Mech.* **189**, 117–134.

Lundbladh, A. & Johansson, A. V. 1991 Direct simulation of turbulent spots in plane Couette flow. *J. Fluid Mech.* **229**, 499–516.

Milinazzo, F. A. & Saffman, P. G. 1985 Finite amplitude steady waves in plane viscous shear flows. *J. Fluid Mech.* **160**, 281–295.

Nagata, M. 1990 Three-dimensional finite-amplitude solutions in plane Couette flow: bifurcation from infinity. *J. Fluid Mech.* **217**, 519–527.

Nayar, N. & Ortega, J. M. 1993 Computation of selected eigenvalues of generalized eigenvalue problems. *J. Comput. Phys.* **108**, 8–14.

Orszag, S. A. & Kells, L. C. 1980 Transition to turbulence in plane Poiseuille and plane Couette flow. *J. Fluid Mech.* **96**, 159–205.

Pugh, J. D. & Saffman, P. G. 1988 Two-dimensional superharmonic stability of finite amplitude waves in plane Poiseuille flow. *J. Fluid Mech.* **194**, 295–307.

Pumir, A., Manneville, P. & Pomeau, Y. 1983 On solitary waves running down an inclined plane. *J. Fluid Mech.* **135**, 27–50.

Reddy, S. C. & Henningson, D. S. 1993 Energy growth in viscous channel flows. *J. Fluid Mech.* **252**, 209–238.

Reichardt, H. 1956 Über die Geschwindigkeitsverteilung in einer geradlinigen turbulenten Couetteströmung. *Z. Angew. Math. Mech.* **36**, 26–29.

Romanov, V. A. 1973 Stability of plane-parallel Couette flow. *Funct. Anal. Applics.* **7**, 137–146.

Saffman, P. G. 1983 Vortices-stability and turbulence. *Ann. N.Y. Acad. Sci.* **404**, 12–24.

Soibelman, I. & Meiron, D. I. 1991 Finite amplitude bifurcations in plane Poiseuille flow: two-dimensional Hopf bifurcations. *J. Fluid Mech.* **229**, 389–416.

Tillmark, N. & Alfredsson, P. H. 1992 Experiments on transition in plane Couette flow. *J. Fluid Mech.* **235**, 89–102.

Waleffe, F. 1995 Transition in shear flows. Nonlinear normality versus non-normal linearity. *Phys. Fluids* **7**, 3060–3066.

Zahn, J. P., Toomre, J., Spiegel, E. A. & Gough, D. O. 1974 Nonlinear cellular motions in Poiseuille channel flow. *J. Fluid Mech.* **64**, 319–345.